

Glass transition in monatomic systems: smearing of the same structure vs two structure competition

Yu. D. Fomin,^{1,2} E. N. Tsiok,¹ V. N. Ryzhov,¹ and V. V. Brazhkin¹

¹ *Institute of High Pressure Physics RAS, 108840 Kaluzhskoe shosse, 14, Troitsk, Moscow, Russia*

² *Moscow Institute of Physics and Technology, 9 Institutskiy Lane, Dolgoprudny City, Moscow Region, Russia*

(Dated: November 15, 2021)

In the present paper we discuss the properties of Voronoi polygons in several monatomic glass-forming systems and compare them with those of the Kob-Andersen mixture. We show that two mechanisms of glass formation are possible: smearing of Voronoi polygons or formation of polygons of two different shapes. Both mechanisms lead to disturbance of the crystalline order in the system and glass transition.

PACS numbers: 61.20.Gy, 61.20.Ne, 64.60.Kw

INTRODUCTION

Glasses are widely used in everyday life and in technology. However, the microscopic mechanisms that give rise to this state of matter remain the subject of controversy: glasses are considered either as simply superviscous liquids, or as a result of a true thermodynamic phase transition to a solid state [1–15]. Glass is a general state of matter, and glass transition is common in many-particle systems. Vitrification is observed on various scales in corpuscular systems, ranging from colloidal suspensions and granular materials to cell cultures. For this reason, understanding this problem is so important to condensed matter science.

In the most general sense, glass transition is a change in a many-body system from an equilibrium liquid state to a nonequilibrium disordered solid state. This change is not a phase transition in the thermodynamic sense, at least not observed in experiments, but is a kinetic phenomenon, in which an amorphous solid does not have time to relax to an equilibrium state on experimental time scales.

In ordinary condensed systems, the structure determines the dynamics: for example, liquids are not ordered, while the molecules move chaotically and relax to an equilibrium thermodynamic state, that is, they lose their connection with the initial conditions. At the same time, crystals are ordered and have a nonzero static shear modulus, while, on average, the positions of the molecules are retained over time. In this case, changes in dynamic behavior follow from changes in the structure caused by thermodynamic phase transitions, liquid - crystal. But glass transition clearly does not fit into this paradigm. Supercooled liquid slows down to a complete stop while maintaining its liquid structure. In this regard, the main question in this area is probably the question of whether the experimentally observed glass transition is a purely dynamic phenomenon in which the liquid stops kinetically, or the observed dynamics is a consequence of the underlying phase transition from an equilibrium liquid to

the state of thermodynamic glass? In the first case, glass is considered simply as a liquid with high viscosity that grows indefinitely with decreasing temperature.

Glass transition temperature T_g in this approach is a purely conditional value corresponding to viscosity values of $10^{12} - 10^{13}$. In a liquid, poise and relaxation times of $10 - 100$ s are comparable to characteristic experimental times (relaxation time corresponds to the average time between hops for each particle). As an example of the dynamic theory of glass transition, we can consider the dynamic facilitation theory [16], associated with one of the main recent achievements in understanding the physics of glass state, the discovery of the phenomenon of dynamic heterogeneity [17–19]. At the moment, neither experiment nor modeling can give a definitive answer as to whether glass transition is inherently a thermodynamic or dynamic phenomenon, which opens up room for theorists to develop new concepts. A deep connection between static and dynamic descriptions is revealed by the theory of random first-order transition (RFOT) [11, 12, 21–23], based on the concept of existence of an exponentially large number of metastable states at dynamic transition temperature T_d that is much higher than T_g , which is the laboratory glass transition temperature.

At temperature T_d , a switch occurs from diffuse dynamics, in which saddle points on the potential energy landscape dominate, to activated dynamics, in which crossings of barriers dominate [19, 20]. The behavior of the system at temperatures above and below T_d is described by the mode-coupling theory (MCT) [24, 25] and RFOT, respectively. In experiments, the crossover is often identified by the transition from Arrhenius to superarrhenius behavior of relaxation times [26, 27]. At temperatures $T > T_d$, transport is largely not collective, and the topology of the state space is unremarkable. However, at $T \rightarrow T_d$, the dynamics slows down and the system gets stuck in a glassy metastable state. At $T < T_d$, there is a huge number of statistically similar glassy metastable states separated by barriers. Since there are so many glassy states, the system will get stuck

in one of the metastable glassy states. In the absence of activated transport, it will remain in this state forever. For this reason, T_d is called a dynamic transition: it is an abrupt transition only for the infinite range model, but in general, it sets a temperature range, in which the dynamics becomes glassy. In addition, at $T < T_d$, dynamic heterogeneity plays an increasingly important role.

One of the facts which make it particularly difficult to study glasses is that usually glass transition takes place in rather complex substances such as network-forming liquids, metallic alloys or organic liquids. At the same time, some works on computer simulation give evidence that even monatomic systems can experience glass transition (see, i.e., Refs. [28, 29, 51, 52]).

It is well known that the structure of a liquid does not undergo very sharp changes during glass transition. The main structural motif of glass transition is splitting of the second peak of the radial distribution function $g(r)$ (RDF). However, even such modest changes are taken into account within MCT and allow predicting glass transition temperature.

A particular class of monatomic systems which can demonstrate glass transition is systems with core-softened potentials. Glass transition in different core-softened models was observed in a number of publications [28, 29, 51, 52]. In particular, in Ref. [32] it was shown that there were some special features of the RDFs of core-softened liquids, which allow predicting their glass-forming ability.

Another class of systems, which demonstrate glass transition, is systems with size polydispersity of particles (see, for instance, Refs [33–35]). It was shown in numerous articles that polydisperse hard spheres [33] or Lennard-Jones (LJ) particles [34, 35] could demonstrate glass transition if the degree of polydispersity was sufficiently large. At the same time, a polydisperse LJ system looks very different from core-softened systems and one can expect that it should vitrify via some other mechanisms.

In the present paper we consider the peculiarities of the microscopic structure of several monatomic systems, which demonstrate glass transition, and compare them with those of a glass-forming binary mixture (the Kob-Andersen (KA) mixture [57]). Based on these results, we show that two different mechanisms are responsible for the failure of system crystallization and its transformation into glass.

SYSTEMS AND METHODS

For this paper we simulated several glass-forming systems by means of a molecular dynamics method. All simulations are performed in the lammmps simulation package [50]. First, we simulated a polydisperse LJ system, i.e., a system with continuous distribution of atomic sizes (pa-

rameter σ of the LJ potential). The size of the particles was taken from the Gaussian distribution with dispersion (the degree of polydispersity) up to $\sigma = 0.2$. A monodisperse LJ system was studied for the sake of comparison. Second, we studied liquid silicon with the Stillinger-Weber (SW) potential specially designed for simulation of amorphous silicon [59]. The third system under investigation was the so-called Repulsive Shoulder System (RSS) [51]. Finally, we simulated a KA mixture, which is a text-book system for investigation of glass transition [57].

In order to prove that the systems under investigation demonstrated glass transition we calculated RDFs, intermediate scattering functions (ISFs), and mean square displacements (MSDs) (see Appendix A for the details of calculations).

The key calculations of this work are related to the investigation of the Voronoi cells of the systems. We calculated the volume of the Voronoi cells and their surface. Using these parameters, we propose a parameter which we call "sphericity":

$$Sp = \frac{(\frac{1}{4\pi}S)^{3/2}}{\frac{3}{4\pi}V}. \quad (1)$$

In the case of an ideal sphere this parameter is equal to unity, i.e., this parameter characterizes the deviation of the cell shape from spherical. Although Voronoi cells cannot be spherical, the different sphericities of cells mean that these cells have a different shape, which is important for characterization of the microscopic structure of liquid or glass. Apparently, the structures with more nearest neighbors have Voronoi polygons with more edges and approach a spherical shape closer than the structures with fewer nearest neighbors. In particular, we calculated the sphericity of an ideal face-centered cubic (FCC) lattice and diamond structure. The corresponding sphericities are $Sp_{FCC} = 1.167$ and $Sp_{diam} = 1.48$.

The sphericity parameter used in the present study is closely related (but not equal) to the 'asphericity' parameter known from the literature [38–44]. The main idea of both parameters is the same: they are equal to unity for a sphere. However, we suppose that the sphericity parameter defined in our paper is more convenient for calculations.

The results for amorphous silicon are expressed in physical units, while the results for all other systems are given in dimensionless units based on the parameters of the interaction potential (see Appendix A for details).

RESULTS AND DISCUSSION

The Polydisperse Lennard-Jones system

In this section we describe the results for the polydisperse LJ particles. Five values of polydispersity are used: $\sigma = 0.0$ (monodisperse particles), $\sigma = 0.05$, $\sigma = 0.1$, $\sigma = 0.15$ and $\sigma = 0.2$.

In order to establish whether a system demonstrates a glass transition we calculate the MSD $\langle r^2(t) \rangle$ and ISFs $F_s(q, t)$ at different temperatures. The magnitude of the wave-vector is $q = 14.04$, which corresponds to the first maximum of the structure factor. Figure 1 shows the equation of state (EOS) of the system for all values of polydispersity. One can see that in the monodisperse system and at $\sigma = 0.05$ the EOS shows a sudden bend which corresponds to the two-phase region of the first-order phase transition. This part of the EOS coincides with the corresponding part of the system phase diagram. At the same time, at higher values of σ the EOS demonstrates a smooth bend. From this result we conclude that the monodisperse system and the system with polydispersity 0.05 crystallize while the systems with higher polydispersity experience glass transition. This conclusion is supported by the calculations of RDFs, MSD and ISFs given in Appendix B.

In order to see the difference in the local structure of these five systems we analyze the properties of the Voronoi polygons at the different values of polydispersity. In all cases we analyze the configurations obtained at temperature $T = 0.1$ which is far below the crystallization or glass transition temperature. Figure 2 (a) shows the distribution of the volume of the Voronoi cells for the systems with different polydispersity. In the case of the monodisperse system the distribution demonstrates a tall narrow peak. As polydispersity increases, the height of the peak decreases and the peak becomes more spread. It corresponds to the smearing of the local structure of the system.

Similar conclusions can be made from the sphericity of the Voronoi cells shown in Fig. 2 (b). It also shows a tall narrow peak in the case of the monodisperse system, which becomes spread in the polydisperse ones.

From this observation we conclude that in the case of the monodisperse LJ system all particles are surrounded by Voronoi cells of similar size and shape, which allows constructing a crystal. At the same time, in the polydisperse systems the volume and shape of the Voronoi cells become widely spread, which prevents the formation of a regular lattice and serves as a mechanism of glass transition in this type of systems.

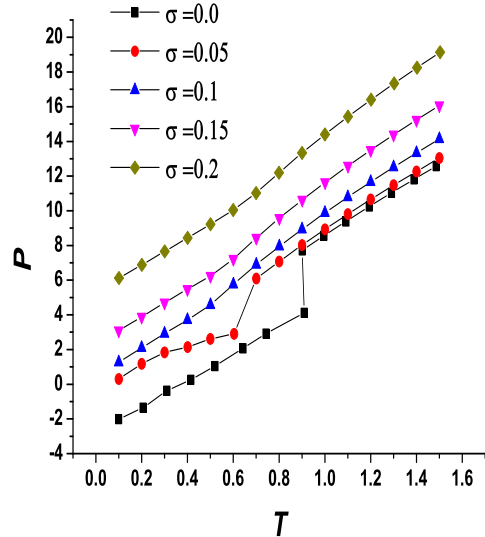


FIG. 1: The equation of state of the polydisperse LJ systems at different values of polydispersity. $\rho = 1.0$.

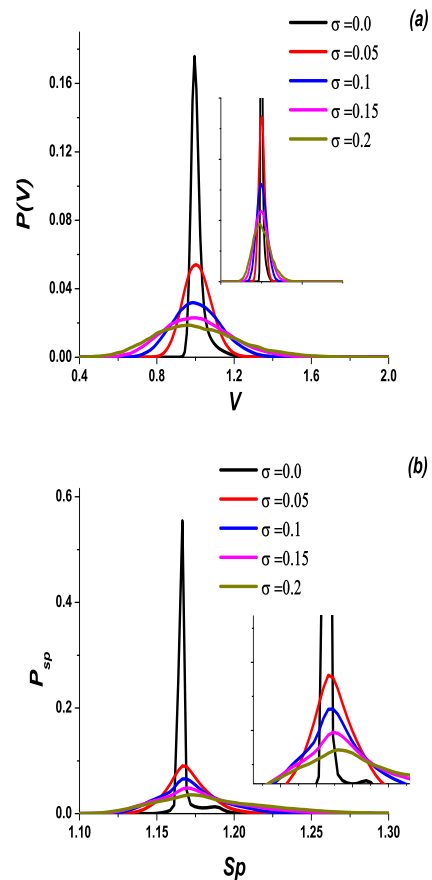


FIG. 2: The distribution of the (a) volume and (b) sphericity of the Voronoi cells of the polydisperse LJ system at different values of polydispersity. $T = 0.1$, $\rho = 1.0$.

Amorphous Silicon

A mechanism responsible for glass transition in the polydisperse LJ system is described above. In order to show that the same mechanism can also take place in other systems we describe here the results for amorphous silicon.

We simulate the behavior of amorphous silicon by the SW potential with the parametrization from Ref. [59], which is specially designed for amorphous silicon. In Ref. [59] it was shown that this potential gave a reasonably good description of the properties of amorphous silicon. At the same time, this model strongly overestimates the melting temperature. We find that at $T = 2000$ K the system spontaneously crystallizes into a diamond lattice. Because of this we do not construct an EOS of this system, but simulate an amorphous state at $T = 800$ K, which should be properly described by the employed model.

The RDFs, MSD and ISFs of this system are given in Appendix B. Figures 3 (a) and (b) show the distribution of the volumes and sphericities of the Voronoi cells for amorphous silicon at $T = 800$ K. One can see that these figures are qualitatively identical to the ones of the polydisperse LJ system, i.e., a spread low peak is observed. Therefore, glass transition in amorphous silicon is related to the smearing of the local structure of particles.

The Repulsive Shoulder System

Another mechanism of glass transition is found in the RSS. Glass transition in this system is described in Refs. [51, 52, 58]. In the present work we also recalculate the MSD and ISFs of this system. The results are given in Appendix B.

Figure 4 shows the distribution of volumes and sphericities of the Voronoi cells of the RSS. One can see that the distribution of volume has a single peak, which, however, demonstrates two shoulders from both left and right sides. At the same time, the distribution of sphericities demonstrates two peaks, i.e., the Voronoi cells are characterized by two different shapes. This result is in agreement with the quasi-binary nature of the system induced by the shape of the interaction potential [51]. Therefore, in the case of the RSS glass transition is induced by a competition of two local structures, which have similar volumes but different shapes. Below we show that the same mechanism is responsible for glass transition in genuine binary mixtures.

The Kob-Andersen mixture

In this section we describe the results for the KA mixture, which is a text-book example of glass-forming liq-

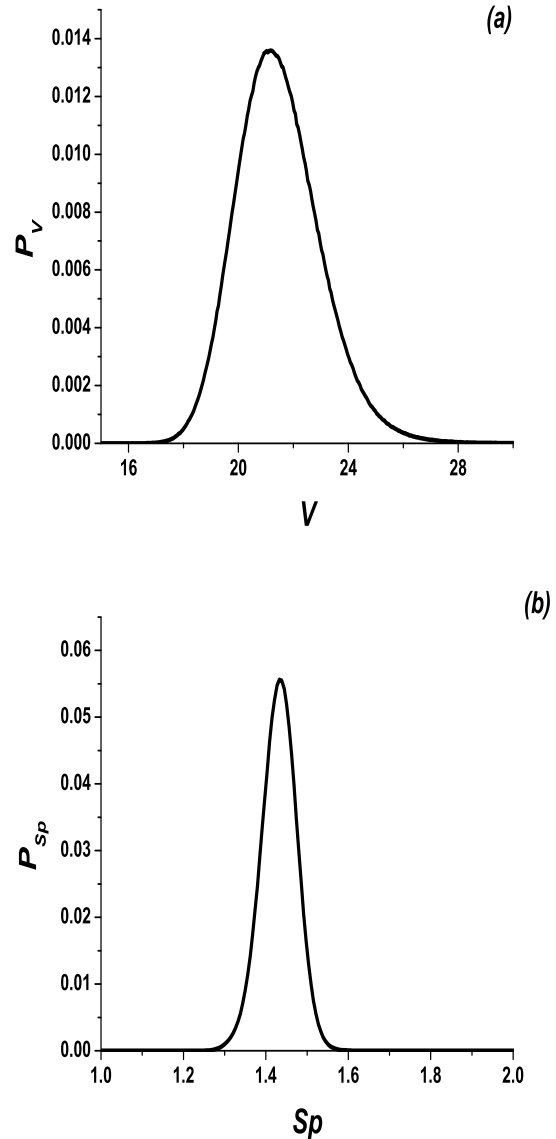


FIG. 3: The distribution of the (a) volume and (b) sphericity of the Voronoi cells of amorphous silicon. $T = 800$ K.

uids. Figure 5 shows the probability distribution of the volumes and sphericities of the KA mixture. One can see that both volumes and sphericities of this system demonstrate two peaks, i.e., the local structures of the Voronoi cells have both different volume and shape. It makes the KA mixture a much better glass-former than the RSS. This result is in agreement with the results of the simulations. Moreover, it proves that a binary mixture is a much better glass-former than a monatomic system, such as an RSS.

In order to compare the results for different systems we make a plot of the probability distribution of sphericity in scaled coordinates: the value of sphericity is scaled

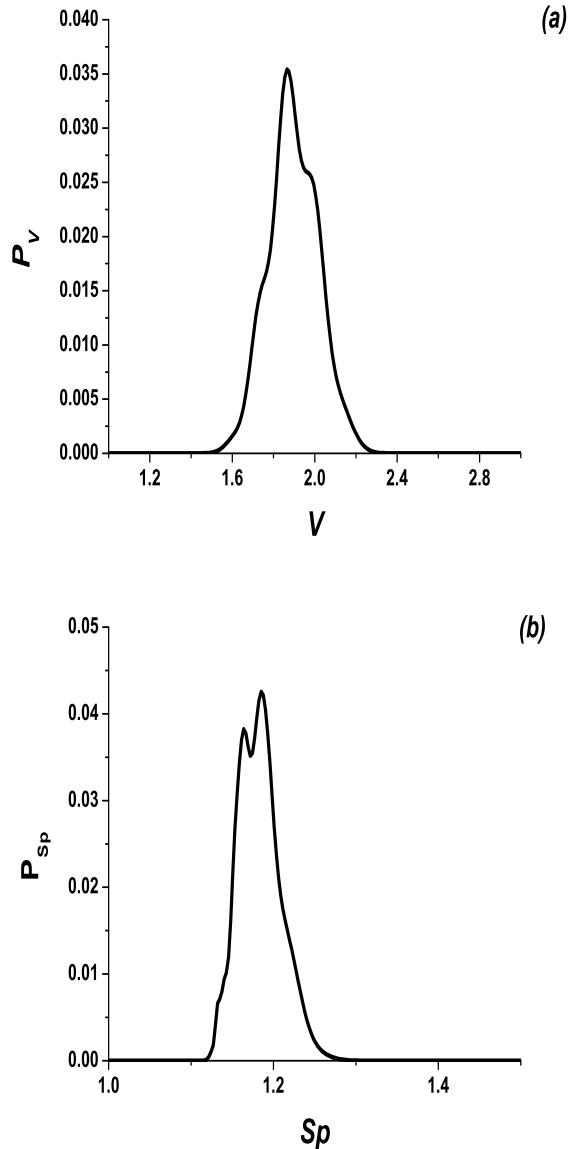


FIG. 4: The distribution of the (a) volume and (b) sphericity of the Voronoi cells of the RSS. $T = 0.06$, $\rho = 0.53$.

to the value of an ideal crystal (1.167 for FCC and 1.48 for the diamond structure) and the distribution itself is normalized to make the height of the peak equal to unity. We compare the width at half-height Γ of the distributions for the different systems. In the case of the RSS the peak is split into two subpeaks above the half-height. We scale the height of the peak on the value of the higher subpeak. In the case of the KA mixture the splitting is more pronounced and the smaller peak is below the half-height. Because of this we use the half-height of the main peak. However, in both cases of the RSS and KA mixture the distribution cannot be approximated by a single peak and values of Γ cannot be strictly compared with

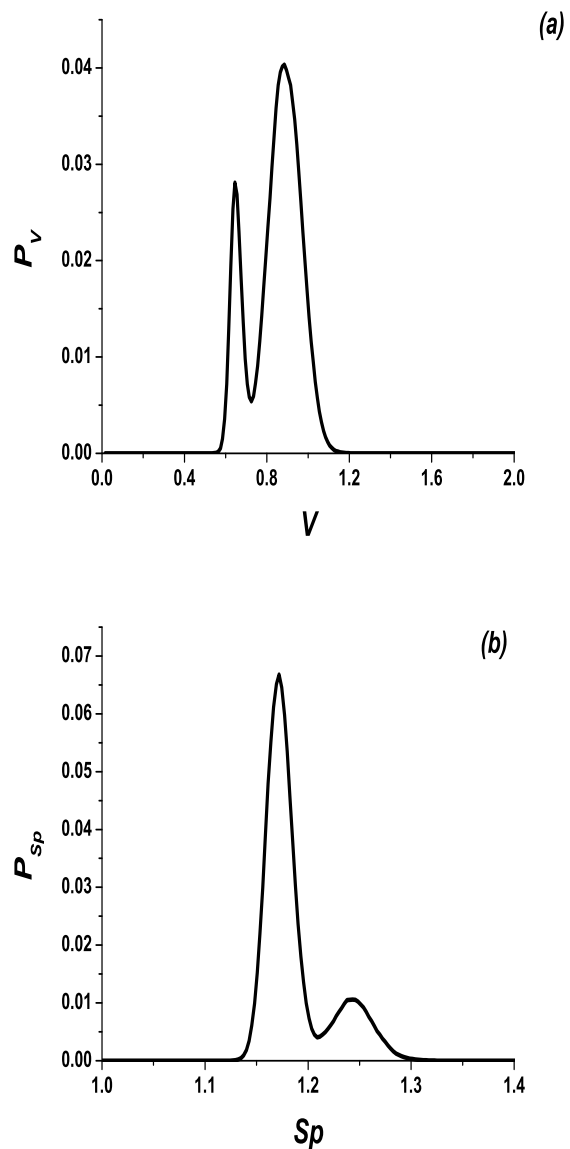


FIG. 5: The distribution of the (a) volume and (b) sphericity of the Voronoi cells of the KA mixture. $T = 0.1$, $\rho = 1.2$.

those of the polydisperse LJ and amorphous silicon.

Figures 6 (a) and (b) confirm the mechanism discussed above. One can see that the width of probability distribution is very small in the case of the pure LJ system, but if the system becomes polydisperse, width Γ rapidly increases. Width Γ is even higher for amorphous silicon, which means that silicon has a strong tendency to amorphization. The width of the probability distribution of the RSS and KA mixture is not a well-defined quantity and we do not discuss it here.

The main arguments of the present study are based on the analysis of the probability distribution of the volumes and sphericities of the Voronoi polyhedra of different sys-

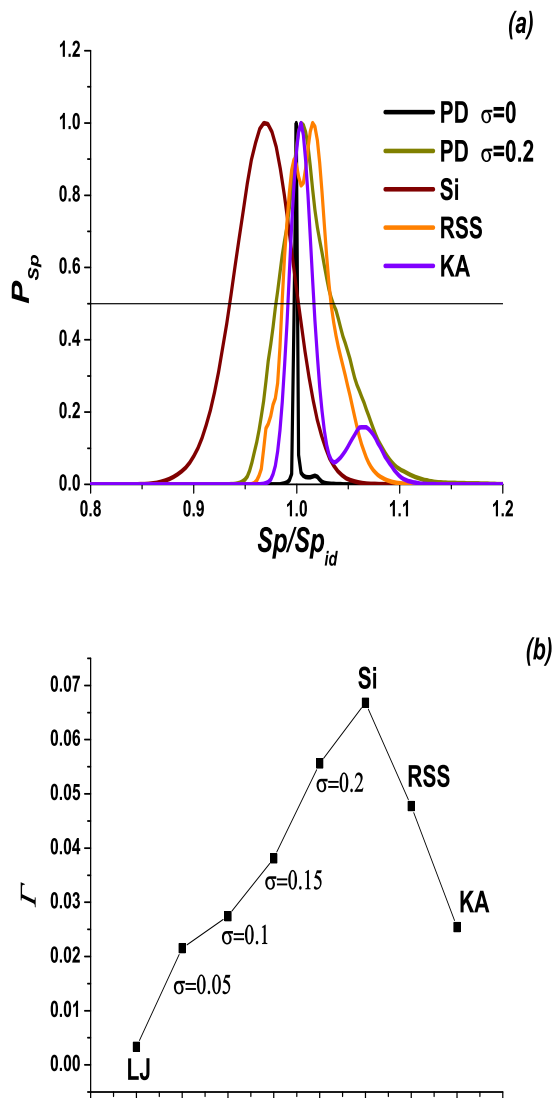


FIG. 6: The probability distribution of sphericities in scaled coordinates: Sp/Sp_{id} , where $Sp_{id} = 1.48$ for amorphous silicon (the diamond structure) and $Sp_{id} = 1.167$ for all other systems (the FCC structure). (b) The width at the half-height of the distribution of different systems (see the text).

tems. Similar analysis of the Voronoi cells of liquids has been performed in a large body of studies, including the Lennard-Jones system [41, 45, 46], water and similar systems (H_2S , HF) [38–40, 43, 44], amorphous silicon [47] and ionic melts [42, 48]. However, all these papers except Ref. [47] deal mostly with the liquid phase and therefore the probability distributions of the properties of Voronoi polyhedra demonstrated a single peak only. Our study showed that the behavior of the probability distribution of the different properties of the Voronoi cells could be

more complex in the case of glassy systems. Importantly, the probability distribution should be accompanied by other characteristics of the system to exclude the possibility of partial crystallization of the system, which could lead to two peak distributions. In the present work we control this by calculating the RDFs, MSDs and ISFs.

CONCLUSIONS

In this paper we analyze the distribution of the volume and shape of the Voronoi cells in several glass-forming systems. We show that two types of the distributions are possible. Some of the glass-formers demonstrate a single but very spread peak of the sphericity parameter. It means that the Voronoi cells of the particles have a wide distribution of shapes, which prevents the crystallization of the system. In some other systems the probability distribution of the sphericity of the Voronoi cells splits into two peaks, i.e., two types of cells appear in the system. From this observation we conclude that two mechanisms of glass formation in monatomic systems are possible: via the spreading of a single local structure and via the splitting of a local structure into two types. This mechanism is also responsible for glass transition in binary mixtures.

These results shed light on the microscopic nature of glass transition in monatomic systems.

This work was carried out using computing resources of the federal collective usage center "Complex for simulation and data processing for mega-science facilities" at NRC "Kurchatov Institute", <http://ckp.nrcki.ru>, and supercomputers at Joint Supercomputer Center of the Russian Academy of Sciences (JSCC RAS). The work was supported by the Russian Science Foundation (Grants No 19-12-00092).

A SYSTEMS AND METHODS

Polydisperse Lennard-Jones particles

The Lennard-Jones potential is defined as

$$U(r) = 4\varepsilon \left(\left(\frac{\sigma_i}{r} \right)^{12} - \left(\frac{\sigma_i}{r} \right)^6 \right), \quad (2)$$

where σ_i is the diameter of the i -th particle. Parameter ε serves as an energy scale.

The diameters of particles are distributed around $\sigma_i = 1.0$ with the Gaussian distribution with dispersion σ . Several values of σ are used: $\sigma = 0.0, 0.05, 0.1, 0.15$ and 0.2 . The simulation setup for all values of polydispersity is the same.

Systems of 32000 particles in a cubic box with periodic boundary conditions (PBC) are used. The time step is set to $dt = 0.001$. The initial structure is obtained as a

high temperature configuration of liquid. Then we equilibrate the systems at temperatures from $T_{min} = 0.1$ to $T_{max} = 1.5$ with a step in temperature $dT = 0.1$ for $5 \cdot 10^7$ steps in the canonical ensemble (constant number of particles N , volume V and temperature T). After that, we perform simulations for more than $5 \cdot 10^7$ steps in a micro canonical ensemble (constant number of particles N , volume V and internal energy E). At this stage we calculate the properties of the system: equation of state (EOS), radial distribution functions (RDF), mean square displacement (MSD) and intermediate scattering functions (ISF). The wave vector for the ISF is chosen as the first maximum of the static structure factor.

Amorphous silicon

In the case of amorphous silicon, a system of 8000 particles is used. The initial configuration is obtained by melting the diamond structure of the system at $T = 8000$ K and $P = 1.0$ bar. Then we simulate the system at constant pressure $P = 1.0$ bar and temperatures from 300 to 1500 K with step 100 K for $1 \cdot 10^7$ steps with time step 1fs.

Additional simulations were performed for temperatures from $T = 2000$ K to 4000 K with step $dT = 500$ K. It was found that at $T = 2000$ K the system spontaneously crystallized. A video of this crystallization is given here. Experimentally the melting point of silicon is 1687 K, which is much below the crystallization point of our simulation. Because of this we think that the model we employ is not valid for high temperature. However, as was shown in Ref. [59] this potential properly described the properties of amorphous silicon. Because of this only the data for the low temperature amorphous phase are discussed in the present paper.

In the isobaric-isothermal simulation we determine the equilibrium density at given temperature. Then we perform simulations in the canonical ensemble for another $1 \cdot 10^7$ steps for equilibration and more $1 \cdot 10^8$ steps in the NVE ensemble for calculation of the properties of the system.

The Repulsive Shoulder System

The Repulsive Shoulder System (RSS) is defined by the potential

$$U(r)/\varepsilon = \left(\frac{\sigma}{r}\right)^{14} + 0.5(1 - \tanh(k(r - \sigma_1))), \quad (3)$$

where parameters ε and σ set energy and length scales, $k = 10.0$ and parameter $\sigma_1 = 1.35$ sets the width of the repulsive shoulder.

The behavior of this system was carefully studied in a number of papers (see Refs. [53–56] and references therein). It was shown that this system demonstrated a very complex phase diagram which strongly depended on parameter σ_1 and numerous water-like anomalies. In particular, in Ref. [51] it was found that at $\sigma_1 = 1.35$ the system experienced glass transition. Later on, this result was confirmed in Ref. [52].

In the present study we simulate a system of 32000 particles in a cubic box with PBC. The initial configuration is high temperature liquid. Then it is infinitely fast quenched to the desired temperature. Firstly, the system is equilibrated in the NVT ensemble for $2 \cdot 10^7$ steps. After that the system is simulated for another $5 \cdot 10^7$ steps in the NVE ensemble for calculation of its properties. The temperatures are from 0.06 to 0.2 with step $dT = 0.01$.

The Kob-Andersen mixture

The Kob-Andersen (KA) mixture is a system of LJ particles of two types, A and B [57]. The interaction parameters are $\varepsilon_{AA} = 1.0$, $\sigma_{AA} = 1.0$, $\varepsilon_{AB} = 1.5$, $\sigma_{AB} = 0.8$, $\varepsilon_{BB} = 0.5$, $\sigma_{BB} = 0.88$. The concentration of A particles is 80%.

We simulate the KA mixture at number density $\rho = N/V = 1.2$, where $N = N_A + N_B$ is the total number of particles in the system. The simulation setup is very similar to that of the polydisperse LJ system. The initial configuration is obtained as high temperature liquid. Then the system is quenched immediately to temperatures $T = 0.1, 0.2 - 1.2$ with step $dT = 0.2$. The system is equilibrated in the NVT ensemble for $2 \cdot 10^7$ steps. More $2 \cdot 10^7$ steps are performed in the NVE ensemble for calculation of properties.

Units

In the case of amorphous silicon, we use physical units of measurements, i.e., temperature is measured in Kelvins, pressure in bars, distance in Angstroms, etc.

In all other cases we use reduced units related to the interaction potential, i.e., parameters ε and σ are used as units of energy and length. All other quantities are expressed in units based on these scales.

B RESULTS AND DISCUSSION

In this section we show the radial distribution functions (RDFs), mean square displacement (MSD) and intermediate scattering functions (ISFs) of the systems under consideration.

The Polydisperse Lennard-Jones system

In this part of the paper, we show the RDFs, MSDs and ISFs of the polydisperse LJ systems with different degrees of polydispersity: $\sigma = 0$ (the monodisperse system), $\sigma = 0.05, 0.1, 0.15$ and 0.2 .

In the case of the monodisperse system the crystallization is easily visible from the behavior of the RDFs (Fig. 7(a)). The MSD and ISFs of this system are given in Fig. 7 (b) and (c).

From the EOS of the system with 5% polydispersity, shown in the main text, we conclude that crystallization takes place at temperature about $T = 0.6$. However, the RDFs of the system remain rather liquid-like even at the lowest temperatures (Fig. 8 (a)). However, crystallization of the system is confirmed by the time correlation functions (TCFs) (Fig. 8 (b) and (c)). As shown in our recent work [58], in the case of crystallization the TCFs experience a jump, while in glass transition they change continuously with temperature. In the present case we do observe a jump. The smearing of the RDFs is related to the formation of numerous small crystallites which do not give a clear crystalline view of the RDFs.

In the case of polydispersity 10% and more both RDFs and TCFs demonstrate glass transition, which can be seen in Figs. 9, 10 and 11.

Amorphous silicon

The radial distribution functions, mean square displacement and intermediate scattering functions of amorphous silicon at two temperatures and ambient pressure are given in Fig. 12 (a)-(c).

The Repulsive Shoulder System

Glass transition in the RSS is first reported in Ref. [51]. Later on, it was confirmed in Ref. [52]. The glass transition temperature in [51] is found to be $T_g = 0.07$. The more elaborate calculations of Ref. [52] report the glass transition temperature to be $T_g = 0.064$.

The lowest temperature of the calculations of this work is $T_{min} = 0.06$, i.e., below glass transition. The RDFs, MSDs and ISFs of this system at $\rho = 0.53$ and a set of temperatures are given in Fig. 13 (a)-(c).

The Kob-Andersen mixture

The radial distribution functions, mean square displacement and intermediate scattering functions of the A type of the KA mixture at $\rho = 1.2$ and a set of temperatures are shown in Fig. 14 (a)-(c).

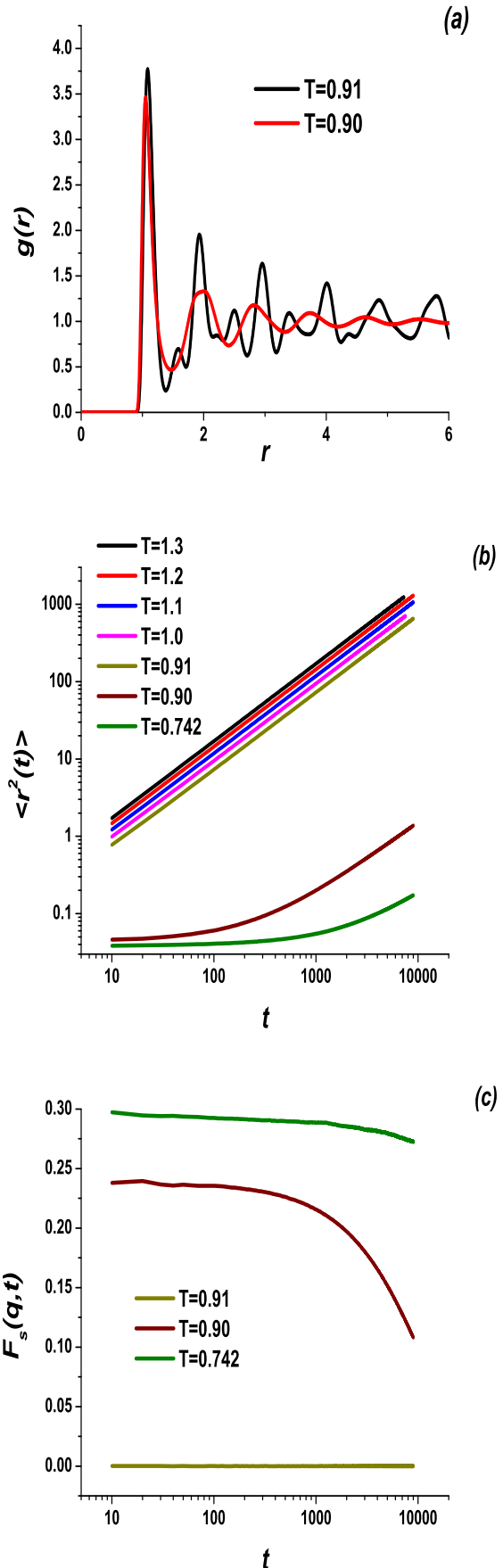


FIG. 7: (a) The radial distribution functions, (b) mean square displacement and (c) intermediate scattering functions of the monodisperse LJ system at $\rho = 1.0$ and a set of temperatures. The wave vector for the ISFs is $k = 1.58$.

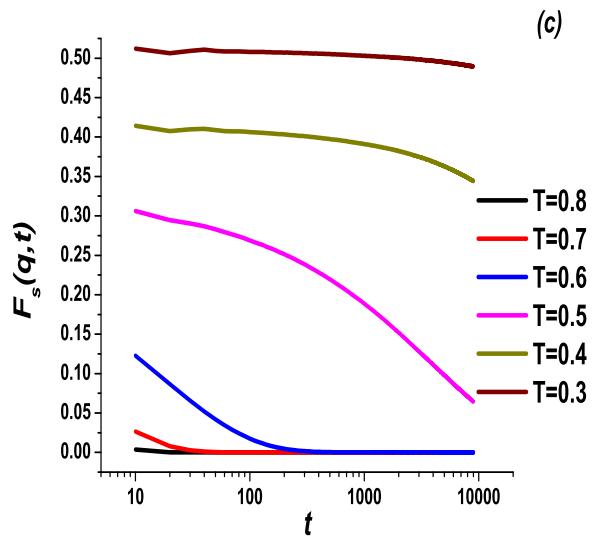
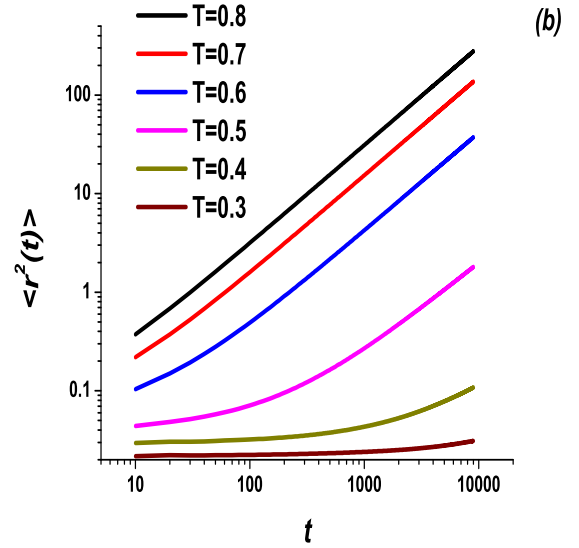
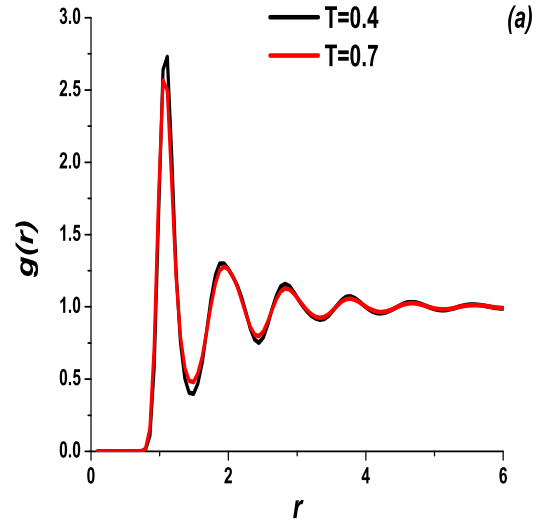
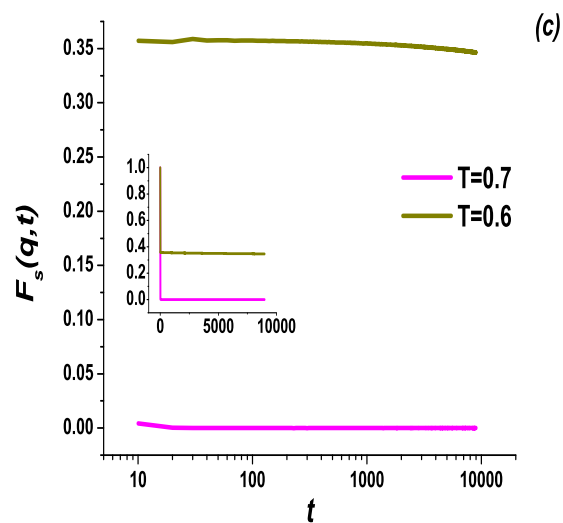
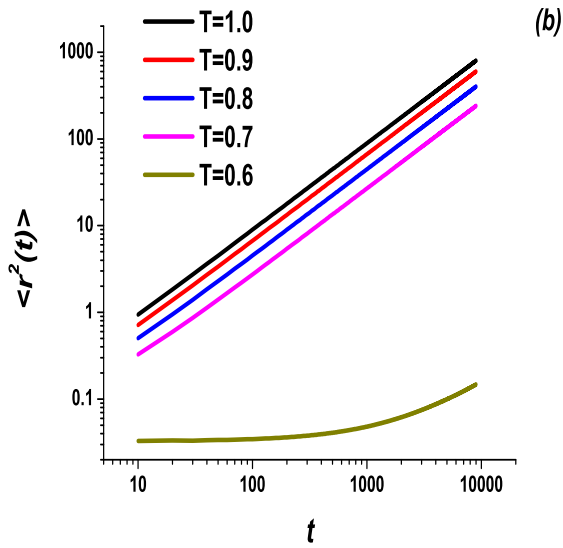
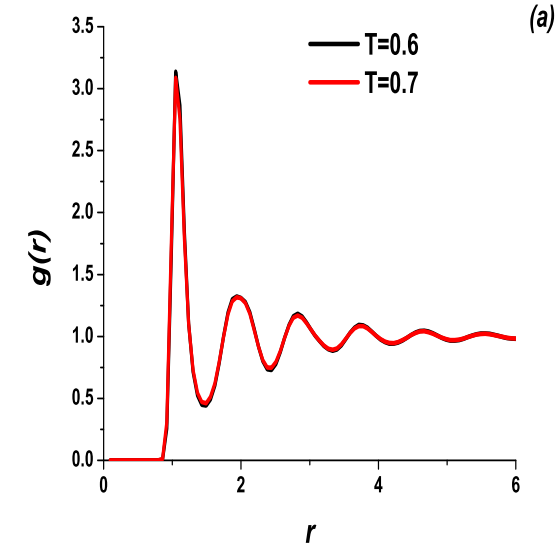


FIG. 8: (a) The radial distribution functions, (b) mean square displacement and (c) intermediate scattering functions of the polydisperse LJ system at $\rho = 1.0$ and a set of temperatures. The degree of polydispersity is 5%. The wave vector

FIG. 9: (a) The radial distribution functions, (b) mean square displacement and (c) intermediate scattering functions of the polydisperse LJ system at $\rho = 1.0$ and a set of temperatures. The degree of polydispersity is 10%. The wave vector

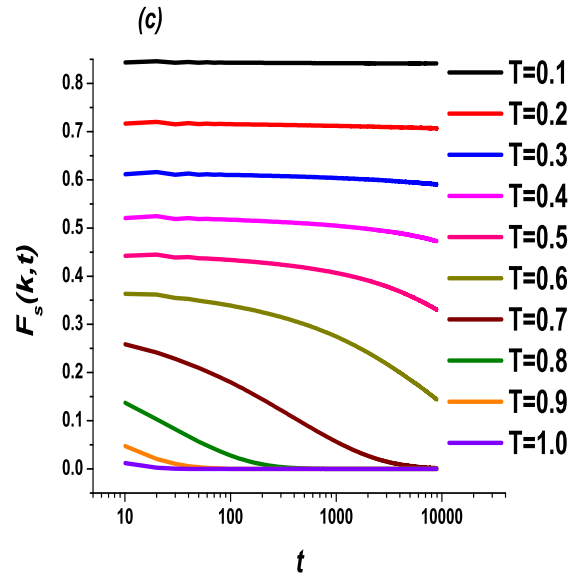
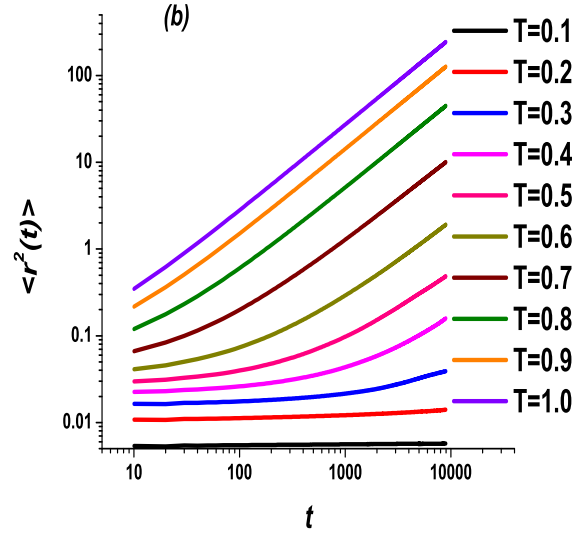
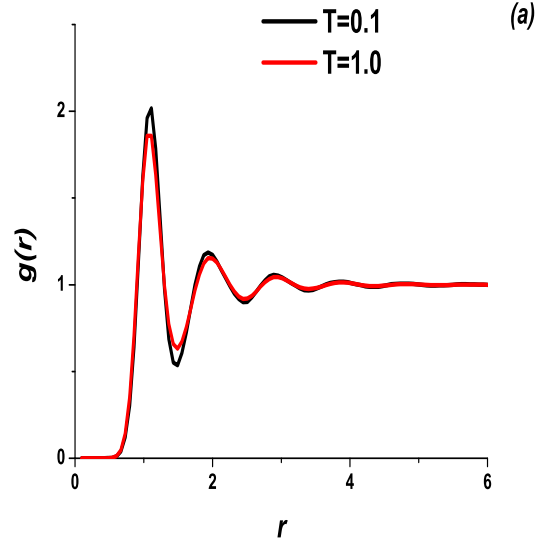
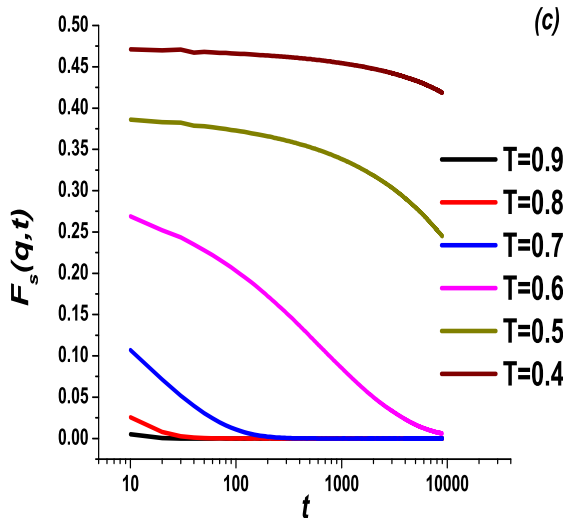
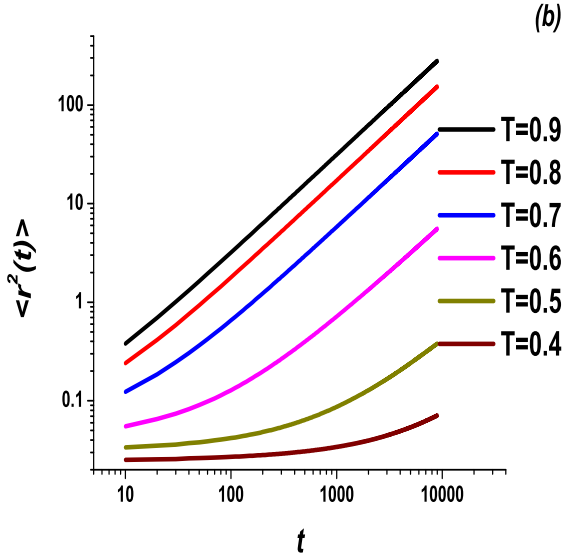
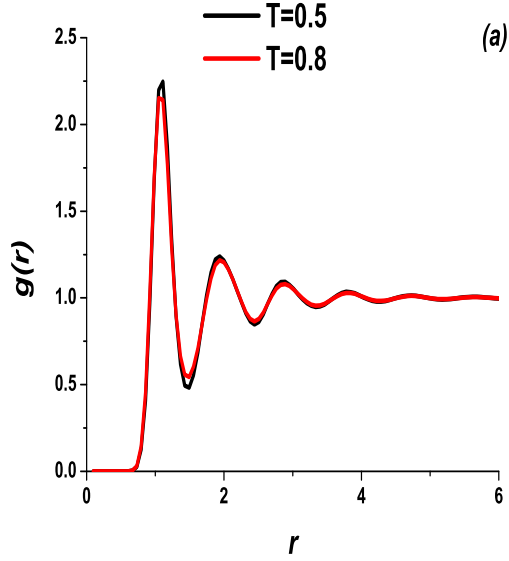


FIG. 10: (a) The radial distribution functions, (b) mean square displacement and (c) intermediate scattering functions of the polydisperse LJ system at $\rho = 1.0$ and a set of temperatures. The degree of polydispersity is 15%. The wave vector for the ISF is $q = 1.5$.

FIG. 11: (a) The radial distribution functions, (b) mean square displacement and (c) intermediate scattering functions of the polydisperse LJ system at $\rho = 1.0$ and a set of temperatures. The degree of polydispersity is 20%. The wave vector for the ISF is $q = 1.5$.

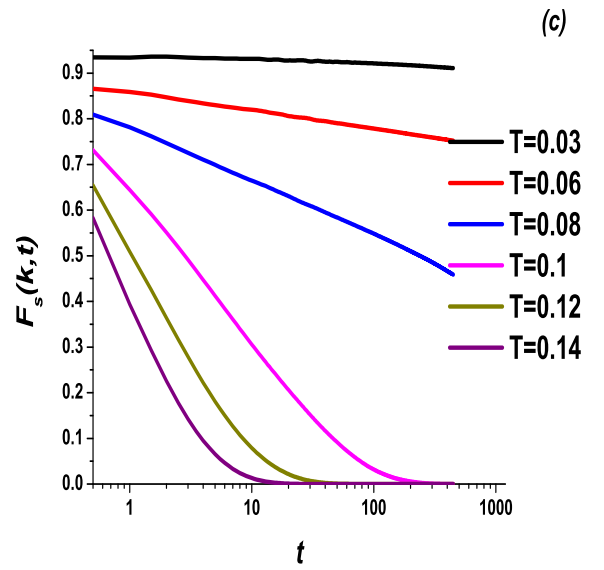
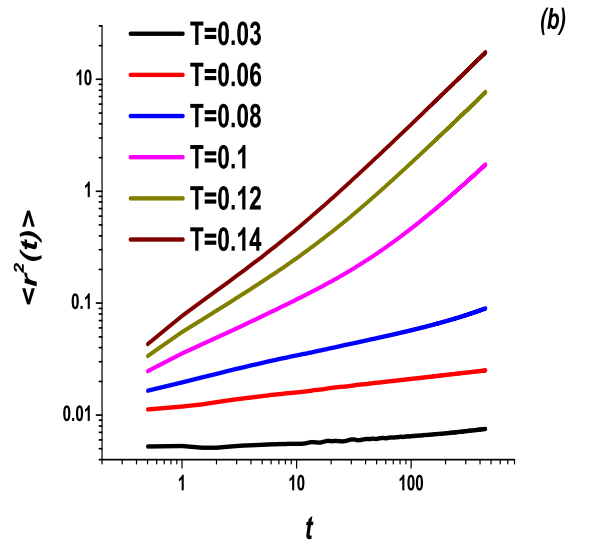
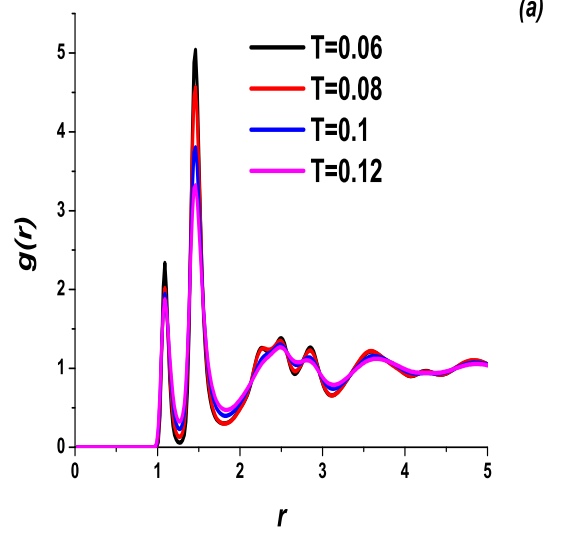
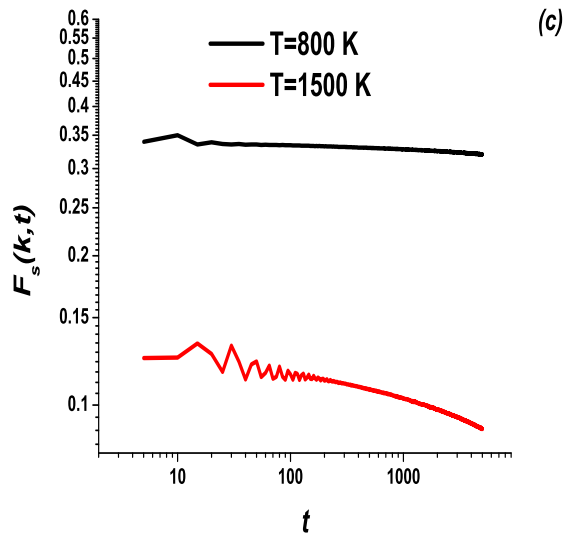
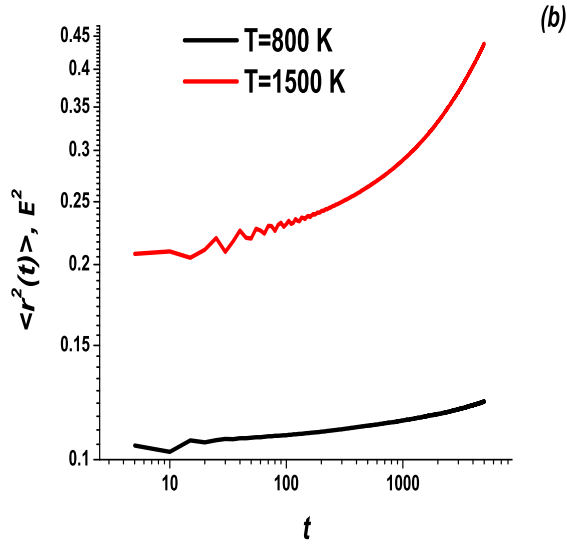
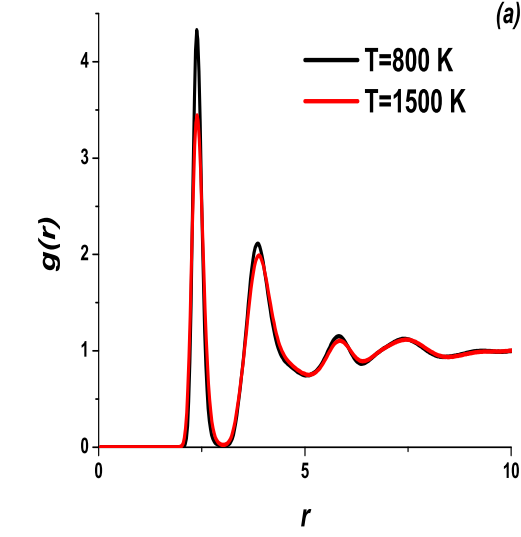


FIG. 12: (a) The radial distribution functions, (b) mean square displacement and (c) intermediate scattering functions of amorphous silicon at two temperatures and ambient pressure. The wave vector for the ISFs is $k = 8.8$.

FIG. 13: (a) The radial distribution functions, (b) mean square displacement and (c) intermediate scattering functions of the RSS at $\rho = 0.53$ and a set of temperatures. The wave vector for the ISFs is $k = 8.8$.

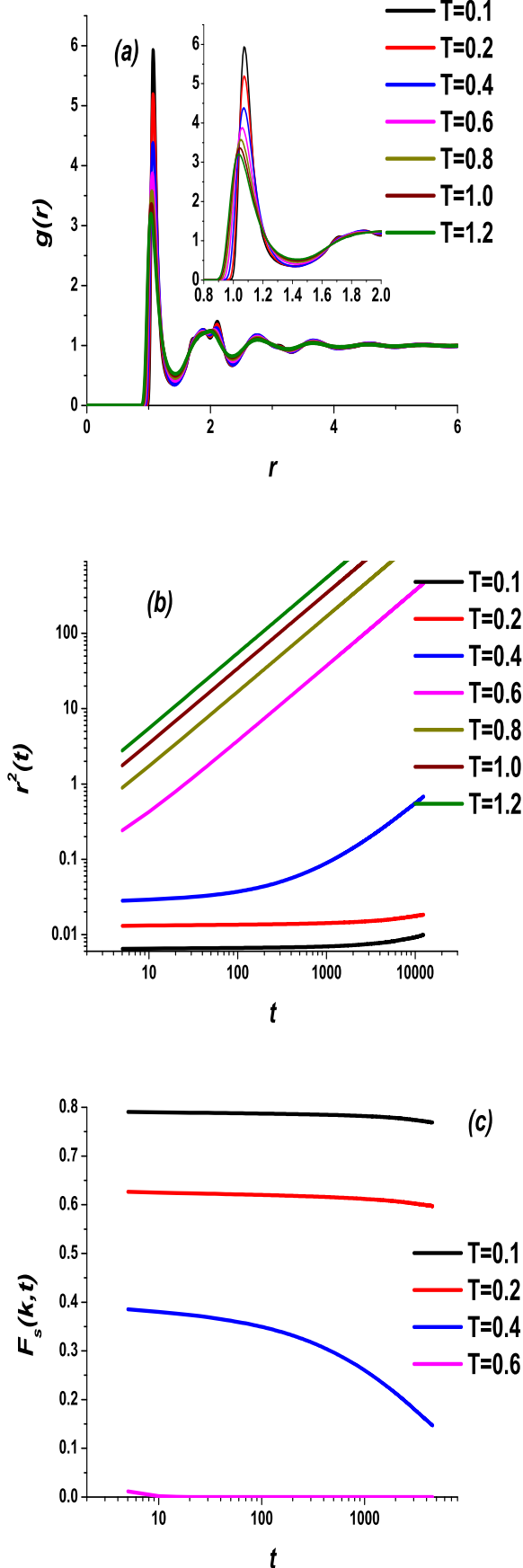


FIG. 14: (a) The radial distribution functions, (b) mean square displacement and (c) intermediate scattering functions of the A type of the KA mixture at $\rho = 1.2$ and a set of temperatures. The wave vector for the ISFs is $k = 14.9$.

- [1] C. A. Angell, *Science* **267**, 1924 (1995).
- [2] M. Ediger, C. Angell, and S. Nagel, *J. Phys. Chem.* **100**, 13200 (1996).
- [3] C. A. Angell, K. L. Ngai, G. B. McKenna, P. F. McMillan, and S. W. Martin, *J. Appl. Phys.* **88**, 3113 (2000).
- [4] P. G. Debenedetti and F. H. Stillinger, *Nature (London)* **410**, 259 (2001).
- [5] V. Lubchenko and P. G. Wolynes, *Annu. Rev. Phys. Chem.* **58**, 235 (2007).
- [6] W. Kob and K. Binder, *Glassy Materials and Disordered Solids: An Introduction to Their Statistical Mechanics*, World Scientific Publishing, 2005, Singapore.
- [7] L. Berthier, and G. Biroli, *Rev. Mod. Phys.* **83**, 587 (2011).
- [8] Jeppe C. Dyre, *Rev. Mod. Phys.* **78**, 953 (2006).
- [9] G. Biroli and J.P. Garrahan, *J. Chem. Phys.* **138**, 12A301 (2013).
- [10] T.R. Kirkpatrick and D. Thirumalai, *Rev. Mod. Phys.* **87**, 183 (2015).
- [11] *Structural Glasses and Supercooled Liquids: Theory, Experiment, and Applications*, edited by P. G. Wolynes, and V. Lubchenko (Wiley, New York, 2012).
- [12] G. Parisi, P. Urbani, F. Zamponi, *THEORY OF SIMPLE GLASSES. Exact Solutions in Infinite Dimensions*, (Cambridge University Press, 2020).
- [13] V.V. Brazhkin, *JETP Letters* **112**, 745 (2020).
- [14] G. Biroli, J.-P. Bouchaud, F. Ladieu, *J. Phys. Chem. B* **125** 7578-7586 (2021).
- [15] S. Albert et al *Science* **352**, 1308 (2016).
- [16] D. Chandler and J.P. Garrahan, *Annu. Rev. Phys. Chem.* **61**, 191 (2010).
- [17] M. D. Ediger, *Annu. Rev. Phys. Chem.* **51**, 99 (2000).
- [18] S. C. Glotzer, *J. Non-Cryst. Solids* **274**, 342 (2000).
- [19] H. C. Andersen, *Proc. Natl. Acad. Sci. U.S.A.* **102**, 6686 (2005).
- [20] S. Sastry, P. G. Debenedetti, F. H. Stillinger, T. B. Schroder, J. C. Dyre, and S. C. Glotzer, *Physica A* **270**, 301 (1999).
- [21] T.R. Kirkpatrick, D. Thirumalai, *Physical Review B* **36**, 5388 (1987).
- [22] T.R. Kirkpatrick, D. Thirumalai, *Physical Review A* **37**, 4439 (1988).
- [23] T.R. Kirkpatrick, D. Thirumalai, P.G. Wolynes, *Physical Review A* **40**, 1045 (1989).
- [24] W. Gotze, *Aspects of Structural Glass Transitions, in Liquids, Freezing and the Glass Transition*, edited by J. P. Hansen, D. Levesque, and J. Zinn-Justin (Elsevier Science, Amsterdam, 1991), pp. 289-502.
- [25] W. Gotze and L. Sjogren, *Relaxation Processes in Supercooled Liquids*, *Rep. Prog. Phys.* **55**, 241 (1992).
- [26] N. Petzold, B. Schmidtke, R. Kahlau, D. Bock, R. Meier, B. Micko, D. Kruk, and E. A. Rossler, *J. Chem. Phys.* **138**, 12A510 (2013).
- [27] D. Coslovich, M. Ozawa, and W. Kob, *Eur. Phys. J. E* **41**, 62 (2018).
- [28] H. Jonsson and H. C. Andersen, *Phys. Rev. Lett.* **60**, 2295 (1988).
- [29] M. Dzugutov, *Phys. Rev. A* **46**, R2984(R) (1992).
- [30] Yu. D. Fomin, N. V. Gribova, V. N. Ryzhov, S. M. Stishov, and Daan Frenkel, *J. Chem. Phys.* **129**, 064512 (2008).

- [31] R. Ryltsev, N. Chtchelkatchev, and V. N. Ryzhov, *Phys. Rev. Lett.* **110**, 025701 (2013).
- [32] R. Ryltsev, B. Klumov, and N. Chtchelkatchev, *Soft Matter* **11**, 6991 (2015).
- [33] E. Zaccarelli, S. M. Liddle, and W. C. K. Poon, *Soft Matter* **11**, 324-330 (2015).
- [34] S. Sarkar, R. Biswas, P. P. Ray, and B. Bagchi, *J. Chem. Sci.* Vol. 127, 1715 (2015)
- [35] Ya. Terada, Th. Keyes, J. Kim, and M. Tokuyama, *AIP Conference Proceedings* 1518, 776 (2013).
- [36] R. L. C. Vink, G. T. Barkema, W. F. van der Weg, N. Mousseau, *J. Non-Cryst. Solids* **282**, 248-255 (2001) .
- [37] W. Kob and H. C. Andersen, *Phys. Rev. Lett.* **73**, 13761379 (1994).
- [38] G. Ruocco, M. Sampoli, and R. Vallauri, *J. Chem. Phys.* **96**, 6167 (1992).
- [39] G. Ruocco, M. Sampoli, A. Torcini, and R. Vallauri, *J. Chem. Phys.* **99**, 8095 (1993).
- [40] J. P. Shih, S. Y. Sheu, and C. Y. Mou, *J. Chem. Phys.* **100**, 2202 (1994).
- [41] J. C. Gil Montoro, and J. L. F. Abascal, *J. Phys. Chem.* **97**, 4211-4215 (1993)
- [42] J. C. Gil Montoro, F. Bresme, and J. L. F. Abascal, *J. Chem. Phys.* **101**, 10892 (1994).
- [43] P. Jedlovsky, *J. Chem. Phys.* **111**, 5975 (1999)
- [44] P. Jedlovsky, *J. Chem. Phys.* **113**, 9113 (2000).
- [45] T.-J. Hsu and Ch.-Yu. Mou, *Mol. Phys.* **75**, 1329-1344 (1992).
- [46] Vladimir P. Voloshin, Yuri I. Naberukhin, Nikolai N. Medvedev, and Mu Shik Jhon, *J. Chem. Phys.* **102**, 4981 (1995).
- [47] V. A. Luchnikov, N. N. Medvedev, A. Appelhagen, and A. Geiger, *Mol. Phys.* **88**, 1337-1348 (1996)
- [48] A. Baranyai and I. Ruff, *J. Chem. Phys.* **85**, 365 (1986).
- [49] Yu. D. Fomin, *Physics and Chemistry of Liquids*, **58**, 290-301 (2020).
- [50] S. Plimpton, *J. Comp. Phys.*, **117**, 1-19 (1995)
- [51] Yu. D. Fomin, N. V. Gribova, V. N. Ryzhov, S. M. Stishov, and Daan Frenkel, *J. Chem. Phys.* **129**, 064512 (2008).
- [52] R. Ryltsev, N. Chtchelkatchev, and V. N. Ryzhov, *Phys. Rev. Lett.* **110**, 025701 (2013).
- [53] N. V. Gribova, Yu. D. Fomin, D. Frenkel and V. N. Ryzhov, *Phys. Rev. E* **79**, 051202 (2009).
- [54] Yu. D. Fomin, V. N. Ryzhov, N. V. Gribova, *Phys. Rev. E* **81**, 061201 (2010).
- [55] Yu. D. Fomin, E. N. Tsiok, and V. N. Ryzhov, *J. Chem. Phys.* **135**, 124512 (2011).
- [56] Yu.D. Fomin, E.N. Tsiok, and V.N. Ryzhov, *Eur. Phys. J. Special Topics* **216**, 165173 (2013).
- [57] W. Kob, H. C. Andersen, *Phys. Rev. Lett.* **73**, 1376 (1994).
- [58] Yu. D. Fomin, *Physics and Chemistry of Liquids* **58**, 290-301 (2020).
- [59] R. L. C. Vink, G. T. Barkema, W. F. van der Weg, N. Mousseau, *J. Non-Cryst. Solids* **282**, 248-255 (2001).